



Cite this: *Nanoscale*, 2018, **10**, 21629

Received 9th October 2018,
Accepted 3rd November 2018

DOI: 10.1039/c8nr08151d

rsc.li/nanoscale

Janus monolayer of WSeTe, a new structural phase transition material driven by electrostatic gating†

Yajing Sun,^a Zhigang Shuai^{a,b} and Dong Wang^{a*}

Phase transition materials are widely exploited in sensors, switches, and information storage devices. However, the dynamic control of structural phase transitions in low-dimensional materials is rarely reported, except for the recent demonstration of semiconductor–semimetal transition in monolayer MoTe₂ modulated by electrostatic gating. Here, based on density functional theory calculations we screen in the Janus family of transition metal dichalcogenides, MXY where M = Mo or W, X/Y = S, Se, or Te, for new two-dimensional phase transition materials. We find that the Janus monolayer of WSeTe undergoes reversible phase transitions modulated by electrostatic gating, owing to the small energy difference between H and T' phases, $E_{T'} - E_H = 48$ meV. The gate voltage of 2.0 V (with high dielectric gating the injected charge is $\sim 10^{13}$ cm⁻²) is required to trigger the semiconductor–semimetal transition in WSeTe. The kinetic barrier for both forward and backward phase transitions is ~ 0.66 eV, which is significantly lower than that in MoTe₂, leading to three orders of magnitude increase in the transition rate and much more rapid response of devices.

Phase transition materials are intriguing for their potential applications in multi-terminal switches, optical devices, electronic oscillators, memory devices, and thermal and chemical sensors.^{1–5} Group VI layered transition metal dichalcogenides (TMDCs) crystallize in both semiconducting H and semimetallic T' phases, and their rich phase-related physics has attracted enormous research interest. In TMDCs except for WTe₂, the thermodynamically stable phase under ambient conditions is the semiconducting H phase, and the T' phases of MoS₂ and MoTe₂ have been fabricated *via* thermal synthesis at high temperatures, elemental substitution, chemical intercalation,

and laser irradiation.^{6–10} The H-to-T' phase transition triggered by these approaches is however irreversible, while physical stimuli including electrostatic gating and straining have been shown to provide a reversible and non-destructive control of the structural phase transition in atomically thin TMDCs.^{11,12} By injection of excessive charges or application of mechanical strains to these materials, the T' phase becomes thermodynamically stable, thus triggering the H-to-T' transition. Once the stimuli are retracted, the reversed T'-to-H transition occurs. Thus, a dynamic control over the crystal phase of TMDCs is achieved. That said, the energy difference between the H and T' phases, $E_{T'} - E_H$, plays an essential role in modulating the phase transition. For example, the energy difference in monolayer MoTe₂ is 36 meV, which is the smallest among the six TMDCs, MX₂ (M = Mo or W; X = S, Se, Te), so a minimal excessive charge of $\sim 10^{14}$ cm⁻² is required to drive the H-to-T' transition in MoTe₂. Recently, such a level of doping was realized in the field-effect transistor (FET) configuration with a high dielectric gating, and reversible structural phase transitions in MoTe₂ monolayers were demonstrated.¹³ For other TMDCs, a much higher level of charge injection is required, so it is difficult to achieve phase transitions by electrostatic doping. In addition to thermodynamics, phase transition kinetics are also important because the sensitivity of devices is determined by how fast such transitions take place. The lower the kinetic barrier E_a , the faster the transition.

In this work, we perform theoretical screening for new phase transition materials, focusing on the Janus monolayers of TMDCs, MXY (M = Mo or W; X, Y = S, Se, or Te). We consider two physical quantities, the phase energy difference and the energy barriers, respectively from perspectives of both thermodynamics and kinetics. The Janus monolayers of MoS₂ have been successfully synthesized either *via* a two-step process involving H₂ plasma stripping and thermal selenization, which replaces the whole layer of S atoms on either side of monolayer MoS₂ with Se atoms, or by controlled sulfurization of monolayer MoSe₂.^{14,15} The synthesis of other types of MXY has not yet been reported, but the techniques established

^aMOE Key Laboratory of Organic Opto Electronics and Molecular Engineering, Department of Chemistry, Tsinghua University, Beijing 100084, P R China. E-mail: dong913@tsinghua.edu.cn

^bKey Laboratory of Organic Solids, Beijing National Laboratory for Molecular Science (BNLMS), Institute of Chemistry, Chinese Academy of Sciences, Beijing 100190, P R China

† Electronic supplementary information (ESI) available. See DOI: 10.1039/c8nr08151d

are equally applicable to most TMDCs. Since the parent materials MoS_2 and MoSe_2 used to synthesize Janus MoSSe are in their thermodynamically stable H phase, thus the prepared MoSSe is also in the H phase, which has been confirmed by transmission electron microscopy, Raman spectroscopy and energy-dependent X-ray photoelectron spectroscopy.^{14,15} The Janus monolayers of MoSSe have been demonstrated to show unique properties arising from their asymmetric atomic structures, including vertical piezoelectric polarization,^{14,16} Rashba spin splitting¹⁷ and high basal plane hydrogen evolution reaction activity.¹⁸ As far as we know, their phase-related properties have never been explored, which we believe may offer new opportunities in their device applications.

The structure of Janus MXY , where M is a group VI-B transition metal atom (Mo and W) and X and Y are different types of chalcogen atoms (S, Se, and Te), was built by replacing one layer of chalcogen atoms X in single-layered MX_2 with chalcogen Y. Thus each monolayer of MXY is composed of a metal layer sandwiched between two chalcogen layers, forming an X-M-Y structure with a three-atom-thick layer. Their H phase exhibits the honeycomb lattice in the atomic plane with three atoms in a hexagonal unit cell, while the T' phase of Janus TMDCs shows distorted octahedral structures with six atoms in an orthorhombic unit cell (Fig. 1a). After the structural optimization, we calculated the energy difference between H and T' phases of all six Janus TMDCs. The results are shown in Fig. 1b in comparison with that of MoTe_2 . Obviously, under ambient conditions the H phase is thermodynamically more stable than the T' phase for all of them. Moreover, the phase energy difference decreases with the increasing atomic mass of chalcogen atoms in both Mo- and W-based Janus monolayers. The $E_{\text{T}'} - E_{\text{H}}$ varies from several tens of meV to several hundreds of meV, with the smallest energy difference of 48 meV per formula unit (f.u.) identified in WSeTe . This value is close to those found in MoTe_2 , 36 meV per f.u. according to our calculations and 31 meV per f.u. or 40 meV per f.u. reported in the literature.^{11,12} So our preliminary screening determines WSeTe to be a potential phase transition material

driven by electrostatic gating. In the following, we took WSeTe as an example to illustrate both thermodynamics and kinetics of the doping induced H-to-T' phase transition process.

The lattice parameters of the H-phase WSeTe are $a = b = 3.405 \text{ \AA}$, and those of the T'-phase are $a = 3.390 \text{ \AA}$ and $b = 6.083 \text{ \AA}$ in the two orthogonal directions, respectively. The height of the Janus monolayer is $h = 3.502 \text{ \AA}$ for the H phase and 3.982 \AA for the T' phase. Previous DFT calculations show that the gate voltage used to drive the H-to-T' phase transition can be arbitrarily reduced in monolayers of $\text{Mo}_x\text{W}_{1-x}\text{Te}_2$ alloys,^{11,12} since the energy difference between H and T' phases can be made arbitrarily small by increasing the composition of heavy W element in the $\text{Mo}_x\text{W}_{1-x}\text{Te}_2$ alloys. Janus TMDCs MXY can be viewed as a special "alloy", with equal compositions of X and Y and ordered structures. We noticed that in the synthesis of the Janus monolayers of MoSSe , $\text{Mo}(\text{S}_{0.5}\text{Se}_{0.5})_2$ alloys with disordered distributions of chalcogen atoms were also created. We then constructed $\text{W}(\text{Se}_{1-x}\text{Te}_x)_2$ alloys with various fractions of Te atoms, and calculated the energy difference between H and T' phases. As shown in Fig. 2, the phase energy difference $\Delta E = E_{\text{T}'} - E_{\text{H}}$ of $\text{W}(\text{Se}_{1-x}\text{Te}_x)_2$

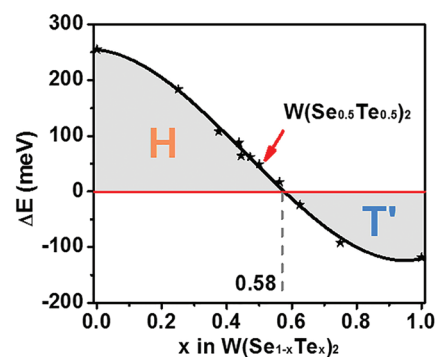


Fig. 2 The phase energy difference $\Delta E = E_{\text{T}'} - E_{\text{H}}$ of $\text{W}(\text{Se}_{1-x}\text{Te}_x)_2$ alloys as a function of Te composition. The H and T' phase boundary is at $x = 0.58$.

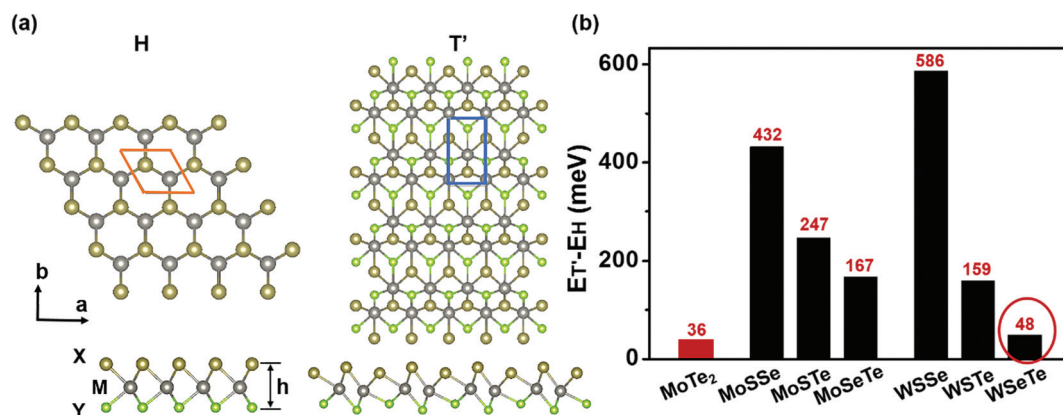


Fig. 1 (a) The top and side views of H phase and T' phase Janus monolayers of MXY , where M = Mo, W; X, Y = S, Se, Te. (b) The phase energy difference $\Delta E = E_{\text{T}'} - E_{\text{H}}$ of MoTe_2 and six Janus monolayers of TMDCs. Among these, the phase energy difference of WSeTe is the smallest and comparable to that of MoTe_2 .

alloys decreases with the increased fraction of Te, and when x exceeds 0.58, the T' phase becomes more stable. At $x = 0.5$, ΔE is 42 meV, almost the same as that in Janus WSeTe. It shows that the energy difference between H and T' phases is not sensitive to the precise atomic structures, instead, it is solely determined by the composition of monolayers.

The Janus monolayer of WSeTe in the H phase is an indirect band gap semiconductor (Fig. 3a). The direct band gap at the K-point is 1.47 eV calculated at the HSE06 level of theory, and the indirect band gap is 1.41 eV between the K-point of the valence band and the M-point (a mid-point along the K- Γ high symmetry line) of the conduction band. The charge density near the valence band maximum (VBM) is localized between W and Se atoms, while that near the conduction band minimum (CBM) resides at the side of Te atoms (Fig. 3b). Such charge separation does not favor the recombination of electrons and holes and was also found in the Janus monolayer of MoSSe.¹⁸ The T' phase is a semimetal, with an energy of 48 meV per f.u. higher than the H phase. Once charges are injected, energies of both phases increased. The energy of the H phase increases more rapidly than the T' phase since excessive electrons will fill the conduction band of the semiconducting H phase, whose energies are significantly higher than the available states around the Fermi level of the semimetallic T' phase (Fig. 3a).

The relative stability of H and T' phases, namely, $\Delta E = E_{T'} - E_H$ as a function of the injected charges is plotted in Fig. 4. Based on thermodynamics, a doping level higher than 0.057 e per f.u. or 0.053 h per f.u. is required to trigger the semiconductor-semimetal transition in WSeTe, and it is comparable to the critical doping level found in MoTe₂ (0.057 e per f.u. or

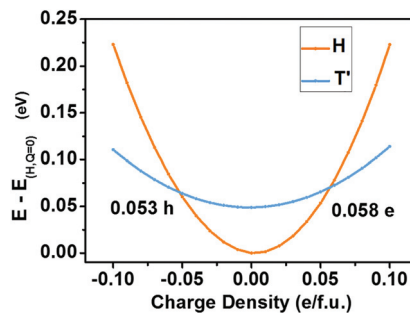


Fig. 4 The energy evolution of H and T' phases of Janus WSeTe as a function of the excessive charge.

0.086 h per f.u.,¹² 0.04 e per f.u. or 0.09 h per f.u.¹¹). This converts to a charge density of $7.2 \times 10^{13} \text{ cm}^{-2}$, which can be achieved in FET devices with high dielectrics. Next, we estimate the critical gate voltage required to trigger the phase transition of Janus WSeTe in the FET device. By using a simple capacitor model, the critical voltage is written as,¹²

$$V = \frac{Q}{C} = \frac{Q}{\epsilon A/t} = \frac{Q t}{A \epsilon}$$

where Q/A is the surface charge density, t is the thickness of the dielectric material (taken as 5 nm HfO₂), $\epsilon = \epsilon_0 \epsilon_r$ with ϵ_0 being the permittivity of vacuum ($8.85 \times 10^{-12} \text{ F m}^{-1}$) and ϵ_r being the relative permittivity of HfO₂ ($\epsilon_r = 25$). The critical gate voltage applied to trigger the phase transition is -2.05 V and 1.91 V for electron and hole injections, respectively.

In addition to thermodynamics, kinetics of the structural phase transition is also interested since it is related to the response time of devices. The nudged elastic band (NEB) method was used to calculate the energy barriers encountered during the forward and backward transitions with the gate voltage turned on or off in the FET configuration. It has been demonstrated that the H-to-T' phase transition occurs with the displacement of chalcogen and metal atoms along the arm-chair direction of the lattice,^{19,20} as illustrated in Fig. 5a. To obtain the kinetic barrier for the H-to-T' transition, we calculated the potential energy curve along the phase transition coordinate, under critical conditions where the excessive charge is 0.057 e per f.u. or 0.053 h per f.u. The energy barrier is 0.659 eV. For the reversed T'-to-H transition, the potential energy curve with the monolayer of WSeTe in the charge neutral state (with the gate voltage switched off) was calculated. The kinetic barrier for the backward transition is 0.657 eV. By assuming the first-order kinetics for the phase transition process, we estimated its rate constant based on Arrhenius' formula $k = \nu \exp(-E_a/k_B T)$, where k is the rate constant, E_a is the energy barrier, k_B is the Boltzmann constant and T is the temperature. ν is the pre-exponential factor, which was taken as the attempted jump frequency in the direction of the phase transition coordinate. The atomic displacement along the phase transition path mentioned above is actually

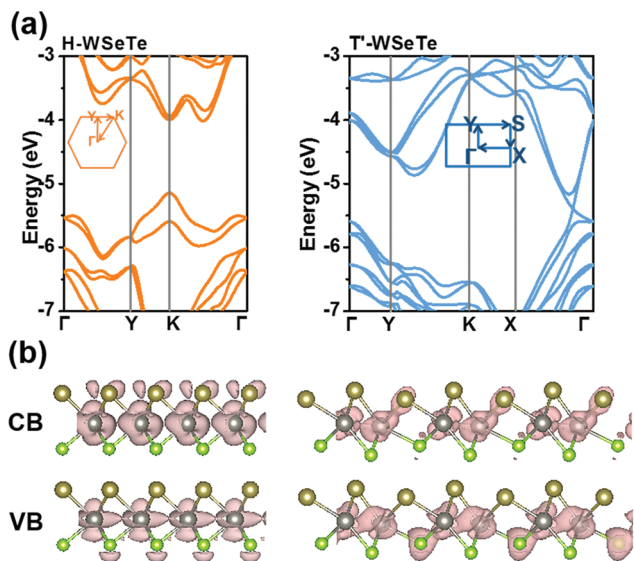


Fig. 3 (a) The band structures of the WSeTe monolayer in the H and T' phases, respectively. (b) The electron densities for electronic states with energies 0–0.4 eV above the CBM and 0–0.4 eV below the VBM of the H phase WSeTe, and those 0–0.1 eV above and 0–0.2 eV below the Fermi level of the T' phase WSeTe.

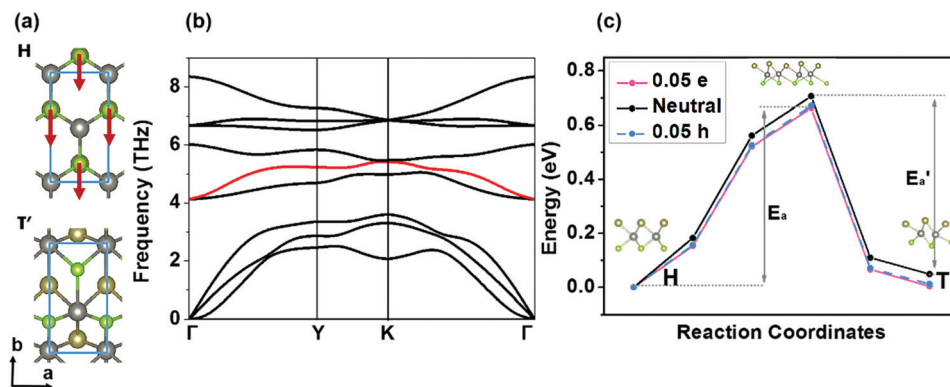


Fig. 5 (a) The atomic displacement during the structural phase transition from the H to the T' phase of WSeTe. (b) The phonon dispersion relation of the H phase WSeTe, with the phonon mode related to the phase transition highlighted in red. (c) The free energy curve along the phase transition path of WSeTe calculated with an excess charge of 0.05 e per f.u. and 0.05 h per f.u. for the H-to-T' transition, and neutral for the T'-to-H transition. The E_a and E'_a represent the kinetic barrier for the forward and backward transitions, respectively.

related to an optical phonon mode marked in red in the phonon dispersion plot (Fig. 5b). We then took this phonon frequency as the attempted jump frequency, which is about $5 \times 10^{12} \text{ s}^{-1}$ in WSeTe. The rate constant is estimated to be 43 s^{-1} . Since the kinetic barriers for the phase transition in WSeTe are hundreds of meV lower than those in MoTe_2 (0.833 eV and 0.830 eV respectively for forward and backward transitions), the transition rate in WSeTe is more than three orders of magnitude higher than that in MoTe_2 at room temperature ($T = 298 \text{ K}$). So, better performance is expected for WSeTe in the sense of device sensitivity.

Conclusions

To conclude, based on DFT investigations of the structural phase transition in the 2D Janus family of Mo- and W-based TMDCs *via* electrostatic doping, we have found the Janus monolayer of WSeTe to be a new phase transition material. The monolayer of MoTe_2 is so far the only 2D TMDC whose structural phase transition has been reversibly modulated, preceded by theoretical predictions, in FET devices with high dielectrics. Our results show that the phase energy difference of the Janus monolayer of WSeTe is as small as 48 meV, comparable to that of MoTe_2 , and a charge injection of 10^{13} cm^{-2} , which corresponds to the gate voltage of $\sim 2.0 \text{ V}$ with HfO_2 dielectrics, is required to enable the room-temperature H-to-T' phase transition. Such a level of charge doping can be easily realized in the FET device. The kinetic barrier for the structural phase transition is lowered, from 0.83 eV in MoTe_2 to 0.66 eV in WSeTe, which results in three orders-of-magnitude increase in the phase transition rate and may substantially improve the sensitivity of devices. Moreover, the phase energy difference of chalcogenide alloy $\text{W}(\text{Se}_{1-x}\text{Te}_x)_2$ with $x = 0.5$ is almost the same as that of WSeTe, indicating that the elemental composition of materials is essential to the phase transition thermodynamics of TMDCs. These findings have expanded our knowledge of phase-related physics of TMDCs,

and will stimulate more innovative research studies towards applications of 2D phase transition materials.

Methods

Density functional theory calculations were performed using the Vienna *Ab Initio* Simulation Package (VASP).^{21,22} The projector-augmented wave (PAW) method was applied with exchange correlation interactions described by the generalized gradient approximation (GGA) using the Perdew–Burke–Ernzerhof (PBE) functional.²³ The initial geometry structure of all six Janus TMDCs MXY was built based on their parent TMDCs in the H and T' phase, respectively. All the structures were optimized after adding a 30 Å vacuum slab along the out-of-plane direction to eliminate interactions between adjacent layers introduced under periodic boundary conditions. A $9 \times 9 \times 1$ Monkhorst–Pack *k*-point mesh in the Brillouin zone and a plane-wave basis cutoff energy of 800 eV were chosen. The criteria of convergence for energy and force were set to be $1 \times 10^{-5} \text{ eV}$ and $0.005 \text{ eV \AA}^{-1}$ respectively. As DFT always underestimated the band gaps, the band structures were also calculated by the HSE06 hybrid functional based on the optimized structure.²⁴ Meanwhile, the spin-orbit coupling and Grimme's dispersion corrections were also considered in our calculations.²⁵ To obtain the energy of a charged Janus monolayer in both H and T' phases, we followed the procedure illustrated in ref. 11 to eliminate the effect of homogeneous background charge added in the vacuum direction in the VASP calculation under periodic boundary conditions. To find the transition state and calculate the phase transition barrier, the nudged elastic band (NEB) method was used.²⁶ The nudged elastic band method is a way to find saddle points and minimum energy paths between the known reactants and products by optimizing a number of intermediate images along the reaction path. In the NEB calculations, the cutoff energy was 800 eV and the ionic relaxation criterion was below 0.02 eV \AA^{-1} . To map atoms between H and T' phases with different symmetries, the orthogonal cell with two formula units was chosen.

Conflicts of interest

There are no conflicts to declare.

Acknowledgements

This work is supported by the National Natural Science Foundation of China (Grant No. 21673123, 21290190, and 91333202) and the Ministry of Science and Technology of China (Grant No. 2015CB655002). Computational resources are provided by the Tsinghua Supercomputing Center.

References

- 1 D. Ruzmetov, G. Gopalakrishnan, C. Ko, V. Narayanamurti and S. Ramanathan, Three-Terminal Field Effect Devices Utilizing Thin Film Vanadium Oxide as the Channel Layer, *J. Appl. Phys.*, 2010, **107**, 114516.
- 2 Q. Gu, A. Falk, J. Wu, L. Ouyang and H. Park, Current-Driven Phase Oscillation and Domain-Wall Propagation in W Nanobeams, *Nano Lett.*, 2007, **7**, 363–366.
- 3 T. Driscoll, H. T. Kim, B. G. Chae, M. Di Ventra and D. N. Basov, Phase-Transition Driven Memristive System, *Appl. Phys. Lett.*, 2009, **95**, 043503.
- 4 B. Kim, Y. Lee, B. G. Chae, S. Yun, S. Oh, H. T. Kim and Y. Lim, Temperature Dependence of the First-Order Metal-Insulator Transition in VO_2 and Programmable Critical Temperature Sensor, *Appl. Phys. Lett.*, 2007, **90**, 023515.
- 5 E. Strelcov, Y. Lilach and A. Kolmakov, Gas Sensor Based on Metal-Insulator Transition in VO_2 Nanowire Thermistor, *Nano Lett.*, 2009, **9**, 2322–2326.
- 6 Y. Cheng, A. Nie, Q. Zhang, L. Gan, R. Shahbazian-Yassar and U. Schwingenschlogl, Origin of the Phase Transition in Lithiated Molybdenum Disulfide, *ACS Nano*, 2014, **8**, 11447–11453.
- 7 K. A. Duerloo, Y. Li and E. J. Reed, Structural Phase Transitions in Two-Dimensional Mo- and W-Dichalcogenide Monolayers, *Nat. Commun.*, 2014, **5**, 4214.
- 8 X. Yin, *et al.*, Tunable Inverted Gap in Monolayer Quasi-Metallic MoS_2 Induced by Strong Charge-Lattice Coupling, *Nat. Commun.*, 2017, **8**, 486.
- 9 J. Young and T. L. Reinecke, Controlling the H to T' Structural Phase Transition Via Chalcogen Substitution in MoTe_2 Monolayers, *Phys. Chem. Chem. Phys.*, 2017, **19**, 31874–31882.
- 10 A. V. Kolobov, P. Fons and J. Tominaga, Electronic Excitation-Induced Semiconductor-to-Metal Transition in Monolayer MoTe_2 , *Phys. Rev. B*, 2016, **94**, 094114.
- 11 Y. Li, K. A. Duerloo, K. Wauson and E. J. Reed, Structural Semiconductor-to-Semimetal Phase Transition in Two-Dimensional Materials Induced by Electrostatic Gating, *Nat. Commun.*, 2016, **7**, 10671.
- 12 C. Zhang, *et al.* Charge Mediated Reversible Metal-Insulator Transition in Monolayer MoTe_2 and $\text{WxMo}_1\text{-Xte}_2$ Alloy, *ACS Nano*, 2016, **10**, 7370–7375.
- 13 Y. Wang, *et al.* Structural Phase Transition in Monolayer MoTe_2 Driven by Electrostatic Doping, *Nature*, 2017, **550**, 487–491.
- 14 A. Y. Lu, *et al.* Janus Monolayers of Transition Metal Dichalcogenides, *Nat. Nanotechnol.*, 2017, **12**, 744–749.
- 15 J. Zhang, *et al.* Janus Monolayer Transition-Metal Dichalcogenides, *ACS Nano*, 2017, **11**, 8192–8198.
- 16 L. Dong, J. Lou and V. B. Shenoy, Large in-Plane and Vertical Piezoelectricity in Janus Transition Metal Dichalcogenides, *ACS Nano*, 2017, **11**, 8242–8248.
- 17 T. Hu, F. Jia, G. Zhao, J. Wu, A. Stroppa and W. Ren, Intrinsic and Anisotropic Rashba Spin Splitting in Janus Transition-Metal Dichalcogenide Monolayers, *Phys. Rev. B*, 2018, **97**, 235404.
- 18 X. Ma, X. Wu, H. Wang and Y. A. Wang, Janus Mosse Monolayer: A Potential Wide Solar-Spectrum Water-Splitting Photocatalyst with a Low Carrier Recombination Rate, *J. Mater. Chem. A*, 2018, **6**, 2295–2301.
- 19 H. H. Huang, X. Fan, D. J. Singh, H. Chen, Q. Jiang and W. T. Zheng, Controlling Phase Transition for Single-Layer MTe_2 ($\text{M} = \text{Mo}$ and W): Modulation of the Potential Barrier under Strain, *Phys. Chem. Chem. Phys.*, 2016, **18**, 4086–4094.
- 20 A. Krishnamoorthy, L. Bassman, R. K. Kalia, A. Nakano, F. Shimojo and P. Vashishta, Semiconductor-Metal Structural Phase Transformation in MoTe_2 Monolayers by Electronic Excitation, *Nanoscale*, 2018, **10**, 2742–2747.
- 21 G. Kresse and J. Furthmuller, Efficient Iterative Schemes for *Ab Initio* Total-Energy Calculations Using a Plane-Wave Basis Set, *Phys. Rev. B: Condens. Matter Mater. Phys.*, 1996, **54**, 11169–11186.
- 22 G. Kresse and J. Furthmuller, Efficiency of *Ab initio* Total Energy Calculations for Metals and Semiconductors Using a Plane-Wave Basis Set, *Comput. Mater. Sci.*, 1996, **6**, 15–50.
- 23 J. P. Perdew, K. Burke and M. Ernzerhof, Generalized Gradient Approximation Made Simple, *Phys. Rev. Lett.*, 1996, **77**, 3865–3868.
- 24 J. Heyd, G. E. Scuseria and M. Ernzerhof, Hybrid Functionals Based on a Screened Coulomb Potential, *J. Chem. Phys.*, 2003, **118**, 8207–8215.
- 25 S. Grimme, J. Antony, S. Ehrlich and H. Krieg, A Consistent and Accurate *Ab Initio* Parametrization of Density Functional Dispersion Correction (Dft-D) for the 94 Elements H-Pu, *J. Chem. Phys.*, 2010, **132**, 154104.
- 26 G. Henkelman and H. Jonsson, Improved Tangent Estimate in the Nudged Elastic Band Method for Finding Minimum Energy Paths and Saddle Points, *J. Chem. Phys.*, 2000, **113**, 9978–9985.